1A2

Polarimetric Radar Remote Sensing

Yoshio Yamaguchi

Department of Information Engineering, Niigata University
Ikarashi 2-8050, Niigata, 950-2181, Japan
yamaguch@ie.niigata-u.ac.jp

1. Introduction

Radar Polarimetry and Polarimetric SAR Interferometry represent the current culmination in '*Microwave Remote Sensing*' technology based on the Antennas, Propagation, Radar and Systems. The purpose and procedure of polarimetry and polarimetric interferometry are shown in Fig. 1. With polarimetric radar sensing, it is possible to carry out 1) detection of targets, 2) decomposition of scattering mechanism, 3) classification of image, much more effectively compared to those of the single polarization radar. By implementing '*radar interferometry*' the spatial (in depth) structure can be explored. With POLInSAR imaging, we can extract tree height for example, which is useful for biomass estimation, or we can monitor the disaster area suffered from earthquake or volcano eruption very precisely. The fundamental data is scattering matrix for polarimetric radar remote sensing. In this presentation, some observation results by Polarimetric Synthetic Aperture Radar (POLSAR) and Polarimetric and Interferometric Synthetic Aperture Radar (POLInSAR) are presented.
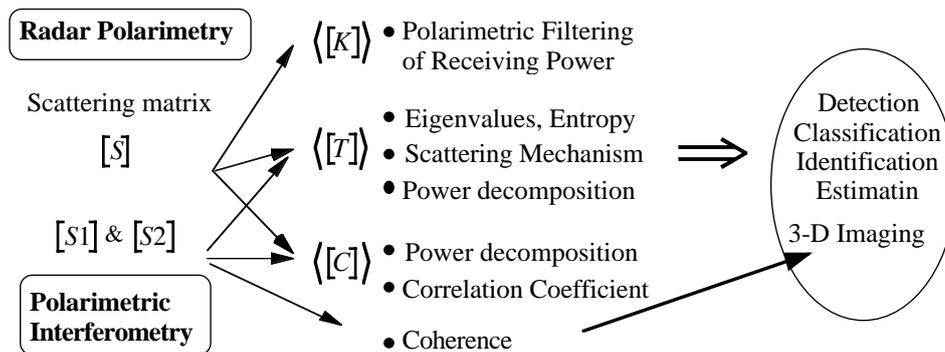

Fig. 1 The purpose and procedure of polarimetry and polarimetric interferometry.

2. What is Radar Polarimetry and Scattering Matrix?

Radar Polarimetry deals with the full vector nature of electromagnetic wave scattered from objects [1]. The scattered wave is represented as

$$\begin{bmatrix} E_H^s \\ E_V^s \end{bmatrix} = [S(HV)] \begin{bmatrix} E_H^t \\ E_V^t \end{bmatrix} = \begin{bmatrix} S_{HH} & S_{HV} \\ S_{VH} & S_{VV} \end{bmatrix} \begin{bmatrix} E_H^t \\ E_V^t \end{bmatrix} \tag{1}$$

where [S] is the scattering matrix, the first subscript letter "H" is used to denote the reception of the Horizontally polarized wave, and the second "V" is for the transmission of the Vertically polarized wave. The radar which acquires scattering matrix is called "Polarimetric Radar". Numerous polarimetric radars are available in the world, starting from hand-made system to air-borne system, and to the space-borne system such as ALOS-PALSAR and TerraSAR-X.

For monostatic radar, the cross-polarized components are identical with each other due to the reciprocity, i.e., $S_{HV} = S_{VH}$. Since the elements are complex valued, we have 6 (for absolute scattering matrix) or 5 (for relative scattering matrix) independent parameters in (2) which represent scattering object. This is the most important point different from those of the single polarization radar.

$$[S(HV)] = \begin{bmatrix} S_{HH} & S_{HV} \\ S_{VH} & S_{VV} \end{bmatrix} \Rightarrow \begin{bmatrix} S_{HH} & S_{HV} \\ S_{HV} & S_{VV} \end{bmatrix} \tag{2}$$

The polarimetric characteristics of target are usually represented in a matrix form whose elements bear the second order statistics such as $\langle S^*_{HH} S_{VV} \rangle$. Ensemble averaging (denoted by symbol $<>$) is necessary to reduce speckle noise in POLSAR image analysis, while keeping the polarization property. Typical polarization matrices are 3 x 3 Covariance matrix $\langle [C] \rangle$, Coherency matrix $\langle [T] \rangle$, and 4 x 4 Kennaugh matrix $\langle [K] \rangle$. The maximum dimension or independent parameter of these polarization matrices becomes 9.

3. What can be done with Scattering matrix?

Once the scattering matrix is obtained, it is possible to synthesize the receiving power as a function of transmitting polarization state of radar wave [2]. The Kennaugh matrix is used to illustrate polarization signature (power pattern). Fig. 2 shows examples of polarization signature of trihedral and dihedral corner reflectors which are often used for polarimetric calibration. The advantage of polarization signature is shape, from which we can estimate unknown scatterer or evaluate the performance of polarimetric calibration under test.
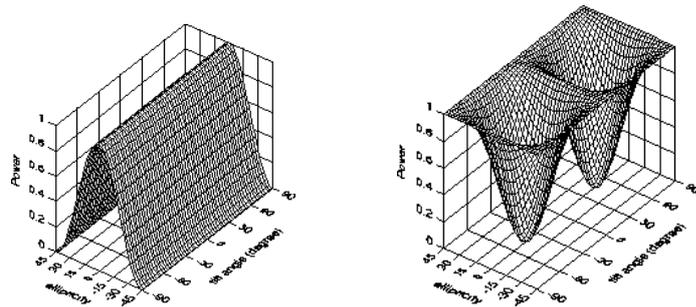

Fig. 2 Polarization signatures: trihedral (left) and dihedral (right) corner reflector.

3.1 Polarimetric Filtering: Enhancement and Elimination of Specific Object

The polarization signature yields the characteristic polarization state of a radar scatterer. For example, the maximum point in the power pattern determines the specific polarization state (ellipticity and orientation angles). This angle set is the characteristic polarization state of the scatterer [3]. If we re-calculate the receiving power using such a polarization state, it is possible to carry out polarimetric filtering of image as shown in Fig. 3.

Enhancement of target   Elimination of surface clutter
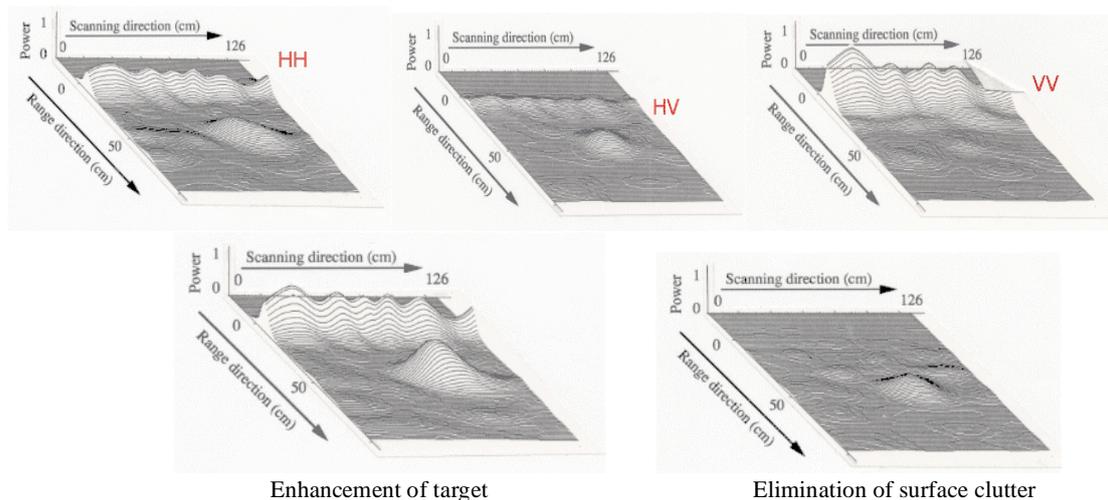
Fig. 3 Examples of polarimetric filtering for ground penetrating radar [4]. The target is buried at 40 cm depth. The upper three images are made directly by scattering matrix data. The lower left shows the maximal enhanced target image using the Co-POL Max polarization state. Although the target is maximized, the surface clutter remains in the image. The lower right shows clutter-suppressed image using the Null polarization state for the surface clutter, resulting in a better contrast (target/clutter) image for GPR. Once the scattering matrix is obtained, it is possible to see image by any polarization combination afterwards.

3.2 Scattering Power Decomposition

Terrain and land-use classification is one of the most important applications of POLSAR sensing. The physical scattering phenomena can be modeled as shown in Fig. 4 where the four-component scattering model [5] (single bounce, double bounce, volume scattering, and helix scattering) is displayed.
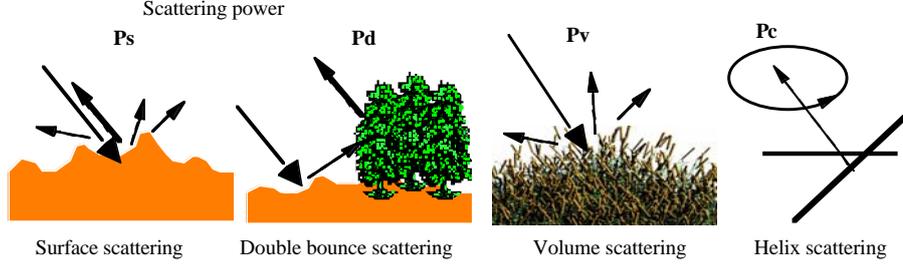

Fig. 4 Scattering powers (*Ps, Pd, Pv*, and *Pc*) associated with physical scattering nature.

Based on these scattering mechanisms, the measured polarization matrices are expanded by the theoretical polarization matrices as follows:

$$\langle [T] \rangle = f_s [T]_{surface} + f_d [T]_{double} + f_v \langle [T] \rangle_{vol} + f_c \langle [T] \rangle_{helix} \tag{3}$$

where f_s, f_d, f_v, *and* f_c are the expansion coefficients. After determining the coefficients by the model fitting, we can derive the corresponding scattering powers (*Ps, Pd, Pv*, and *Pc*). As an example of the scattering power decomposition, Fig. 5 shows the decomposed image of disaster area (the former Yamakoshi village, Japan) suffered from a great earthquake. The data set was acquired with the airborne "Pi-SAR" system developed by NiCT/JAXA, Japan, on Oct. 26, 2004, in rainy condition. For the sake of comparison, an aerial photo is provided. It is seen that residential houses and man-made structures can be recognized clearly by Red and Yellow colors in the decomposition image [6].
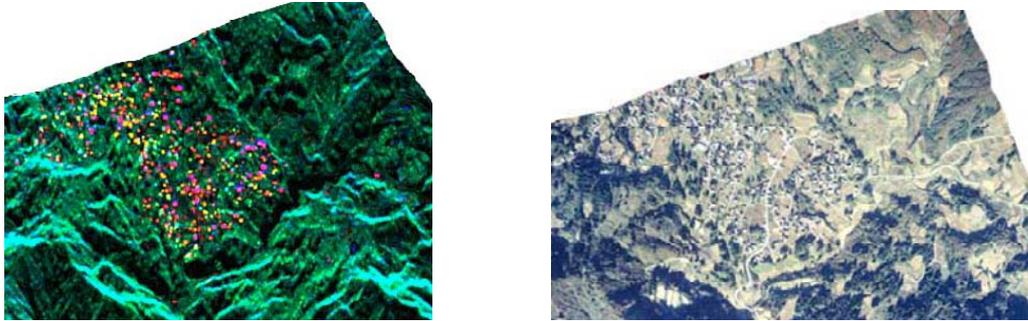
(a) Color-coded decomposed X-band Pi-SAR image (b) Precinct of Yamakoshi village, Niigata, Japan by photo

Fig.5 Comparison with SAR image and Photo. Color-code is used for indication: Volume scattering (Green) from trees and vegetations, Double bounce scattering (Red) from man-made structures, Surface scattering (Blue) or single bounce scattering.

3.3 Polarimetric Correlation Coefficient

The correlation coefficient is also an important polarimetric index for classifying scattering objects. Since the elements of covariance matrix are directly related to correlations, the investigation on the covariance matrix serves the classification purpose. It is known from the experimental observations that the cross-correlations are close to zero for natural distributed target, i.e., $\langle S_{HH} S_{HV}^* \rangle \approx \langle S_{VV} S_{HV}^* \rangle \approx 0$, and are non-zero for man-made structures. In addition, the correlation coefficient in the Left and Right circular polarization basis (LR) has been found to be useful for finding azimuthal slope detection [7] and man-made scatterer [8]. It can be expressed in terms of scattering matrix elements in the HV polarization basis as

$$\gamma_{LL-RR} = |\gamma_{LL-RR}| \angle \varphi_{LL-RR} = \frac{\langle 4|S_{HV}|^2 - |S_{HH} - S_{VV}|^2 \rangle - j4\,\mathrm{Re}\langle S_{HV}^*(S_{HH} - S_{VV})\rangle}{\sqrt{\langle |S_{HH} - S_{VV} + j2S_{HV}|^2 \rangle \langle |S_{HH} - S_{VV} - j2S_{HV}|^2 \rangle}} \tag{4}$$

The correlation coefficient was applied to examine Pi-SAR image data around Niigata University, and the ground structure level was recovered as shown in Fig. 6.
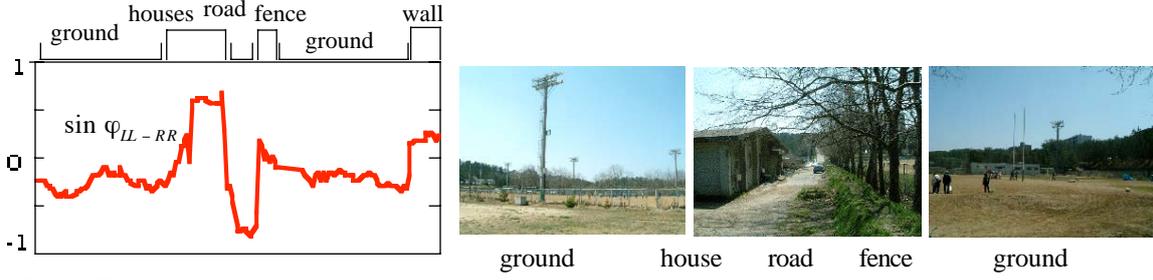

Fig. 6 The phase information and the corresponding ground structure along a transect in Niigata University.

3.4 Eigenvalue Analysis: Entopy, Angle Alpha, Anisotropy / Total power

Cloude and Pottier [9] have developed the Entropy based decomposition. The coherency matrix is expanded as a sum of eigenvalues and eigenvectors.

$$\langle\, [\,T\,]\,\rangle = [\,U_3\,] \begin{bmatrix} \lambda_1 & 0 & 0 \\ 0 & \lambda_2 & 0 \\ 0 & 0 & \lambda_3 \end{bmatrix} [\,U_3\,]^\dagger = \sum_{i=1}^{3} \lambda_i\, e_i\, e_i^\dagger \qquad (5)$$

Using the eigenvalues λ_i, the following parameters are defined.

$$\text{Probability: } P_i = \frac{\lambda_i}{\lambda_1 + \lambda_2 + \lambda_3} \,(\,i = 1, 2, 3\,), \quad \text{Entropy: } H = -\sum_{i=1}^{3} P_i \log_3 P_i \,(\,0 \le H \le 1\,) \qquad (6)$$

$$\text{Angle alpha } \bar{\alpha} = \sum_{i=1}^{3} P_i\, \alpha_i \,(\,0° \le \bar{\alpha} \le 90°\,), \quad \text{Anisotropy: } A = \frac{\lambda_2 - \lambda_3}{\lambda_2 + \lambda_3}, \quad \text{Total Power: } TP = \lambda_1 + \lambda_2 + \lambda_3 \qquad (7)$$

Based on the above parameters, various POLSAR images have been analyzed [10]-[12], including urban area, forest area, glacier, and ocean.

4. What is Polarimetric Interferometry?

The fundamental idea of interferometry consists of an accurate phase analysis of the radar waves backscattered from object. Two receiving antennas, placed in different locations, are used for interferometry. This separation (baseline) can be accomplished by repeat pass flight by spaceborne radar. Whereas simple interferometry is concerned with single fixed polarization data, polarimetric interferometry uses fully polarimetric data, i.e., a pair of scattering matrices to retrieve better phase information. Using two scattering matrices, optimal coherence can be extracted, which in turn produces detailed and accurate phase information of the scatterer. There are several methods to obtain "coherence" [13]-[15]. From which we can reconstruct tree height which is essential for biomass estimation. Fig. 7 shows one example of tree height estimated by POLInSAR by Yamada [14].
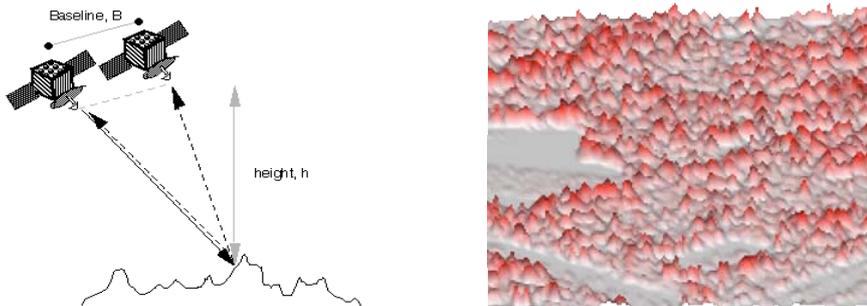

Fig. 7 The basic principle of Polarimetric SAR Interferometry and tree height estimation

5. POLSAR Applications to Environmental Sensing

We applied the scattering power decomposition technique for monitoring seasonal changes of wetland area. The site is located at 37º49'N 138º53'E in Niigata Prefecture, Japan, where a small lagoon named *"SAKATA"* has been registered as a RAMSAR site (one of 33 sites in Japan) according to the Convention on Wetlands of International Importance especially as Migratory Waterfowl Habitat (Ramsar Treaty). Using high resolution Pi-SAR L- and X- band data, the 4-component decomposition was carried out to see seasonal changes as shown in Fig. 8. The characteristic feature is that color (scattering mechanism) changes season by season. In the middle of the lagoon, we see Red (double bounce scattering power) in the L-band data on 2004.8.4. This is caused by double bounce structure consisting of stem of Lotus and water surface. On the other hand, it turned out to be Blue (single bounce power) in the X-band. The difference in color indicates the difference of scattering mechanisms. Since the L-band wave can penetrate deeper into vegetation, it is reflected from inside. The X-band wave is backscattered from canopy surface of vegetation. As season changes, the color changes according to the growing and withering status of vegetation. This kind of information reveals that the environmental situation of vegetation.
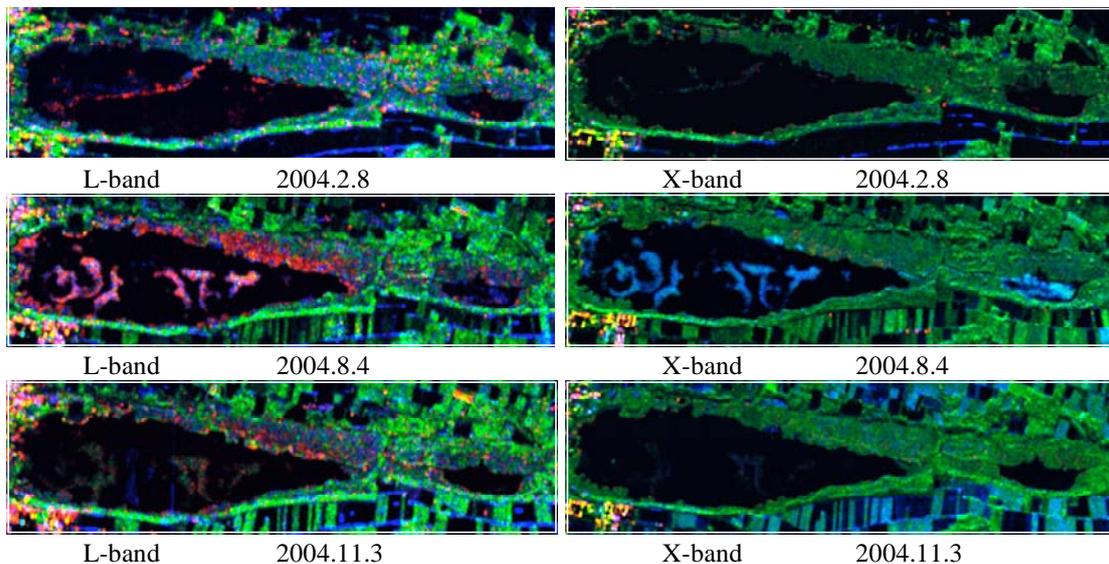

L-band	2004.2.8	X-band	2004.2.8
L-band	2004.8.4	X-band	2004.8.4
L-band	2004.11.3	X-band	2004.11.3

Fig. 8 Color-coded composite image of decomposed powers of *SAKATA* area: Red (double bounce scattering power), Green (volume scattering power), Blue (single bounce power).

6. Spaceborne Mission

Several airborne POLSAR systems such as AIRSAR, E-SAR, Pi-SAR, etc. have demonstrated the usefulness and advantages of fully polarimetric SAR data compared to the conventional single or dual polarization SAR data. Based on the experimental airborne SAR observations, JAXA, Japan, had launched the first space-borne L-band fully polarimetric SAR system named "PALSAR" on Jan. 24, 2006. TerraSAR-X (Germany) and RadarSAT-2 (Canada) data will soon be available. Since the orbit in space is quite stable, high quality POLSAR and POLInSAR data will come out and serve for environmental remote sensing.

ALOS-PALSAR (L-band)　　　　TerraSAR-X (X-band)　　　　RadarSAT-2 (C-band)

Fig. 9   Space-borne fully polarimetric radar system

7. Concluding Remarks

In this paper, a brief introduction of Polarimetric Radar is given with a great expectation that the advantages of fully polarimetric data and the performances as well as the importance are recognized. All of the items shown here cannot be accomplished without fully polarimetric data. A considerable database of fully polarimetric data by space-borne systems will become available in the very near future. The POLSAR and POLInSAR data will serve remote sensing technology development much more effectively compared to the single polarization radar data. The research on the data utilization including science, methodology, algorithm, validation, as well as worldwide community network will serve the environmental protection of the planet Earth.

Acknowledgments

References

[1] F. M. Henderson, A. J. Lewis, Principles & Applications of Imaging Radar, Manual of Remote Sensing, 3rd ed., vol. 2, ch. 5, pp. 271-357, John Wiley & Sons, Inc, 1998.

[2] J. J. van Zyl, H. A. Zebker, C. Elachi, "Imaging radar polarization signatures: Theory and Observation," *Radio Science*, vol.22, no.4, pp.529-543, 1987.

[3] W. -M. Boerner, W. L. Yan, A. -Q. Xi, and Y. Yamaguchi, "On the basic principles of radar polarimetry: The target characteristic polarization state theory of Kennaugh, Huynen's polarization fork concept, and its extension to the partially polarized case," *Pro. of the IEEE*, vol. 79, no. 10, pp. 1538-1550, Oct. 1991

[4] T. Moriyama, Y. Yamaguchi, H. Yamada, and M. Sengoku, "Reduction of surface clutter by a polarimetric FM-CW radar in underground detection," *IEICE Trans. Communications*, vol. E78-B, no. 4, pp. 625-629, April 1995

[5] Y. Yamaguchi, T. Moriyama, M. Ishido, and H. Yamada, "Four-component scattering model for polarimetric SAR image decomposition," *IEEE Trans. GRS,* vol. 43, no. 8, pp. 1699-1706, Aug. 2005.

[6] Y. Yamaguchi, "On the utilization of fully polarimetric data in radar polarimetry," *Trans. of IEICE*, vol. J89-B , no.9, pp. 1539-1547, 2006 (in Japanese)

[7] D. L. Shuler, J. S. Lee, G. DeGrande, "Measurement of topography using polarimetric SAR images," *IEEE Trans. GRS,* vol. 34, no. 6, pp. 1266-1277, 1996.

[8] K. Kimura, Y. Yamaguchi, H. Yamada, "Circular polarization correlation coefficient for detection of non-natural targets aligned not parallel to SAR flight path in the X-band POLSAR image analysis," *IEICE Trans. Commun.,* vol. E87-B, no. 10, pp. 3050-3056, Oct. 2004.

[9] S. R. Cloude, and E. Pottier, "An entropy based classification scheme for land applications of polarimetric SAR," *IEEE Trans. GRS,* vol. 35, no. 1, pp. 68-78, Jan. 1997.

[10] E. Pottier, "Unsupervised classification scheme and topography derivation of POLSAR data based on $<<H/A/\alpha>>$ polarimetric decomposition theorem," in Proc. 3rd Int. Workshop Radar Polarimetry, pp. 106-111, 1995.

[11] L. S. Lee, et al., "Unsupervised classification using polarimetric decomposition and the complex Whishart classifier," *IEEE Trans. GRS*, vol. 37, pp. 2249-2258, Sep. 1999.

[12] K. Kimura, Y. Yamaguchi, H. Yamada, "Unsupervised land classification using $H/\alpha/TP$ space applied to POLSAR image analysis," *IEICE Trans. Commun.,* vol. E87-B, no. 6, pp. 1639-1647, June 2004.

[13] S. R Cloude, K. Papathanassiou, E. Pottier, "Radar Polarimetry and Polarimetric Interferometry," *IEICE Trans.,* vol. E84-C, no. 12, pp. 1814-1823, Dec. 2001.

[14] H. Yamada, Y. Yamaguchi, et al., "Polarimetric SAR interferometry for forest analysis based on the ESPRIT algorithm," *IEICE Trans. Electron.*, vol. E84-C, pp. 1917, 1924, 2001.

[15] H. Yamada, M. Yamazaki, Y. Yamaguchi, "On Scattering model decomposition of PolSAR image and its application to the ESPRIT-based Pol-inSAR", *EUSAR 2006* (6th European Conference on Synthetic Aperture Radar), May 2006.